Atmospheric correction in presence of sun glint: application to MERIS

François Steinmetz, Pierre-Yves Deschamps and Didier Ramon

HYGEOS, Euratechnologies, 165 avenue de Bretagne, 59000 Lille, France

fs@hygeos.com

Abstract: The sun glint is a major issue for the observation of ocean color from space. For sensors without a tilting capacity, the observations at sub-tropical latitudes are contaminated by the bright pattern of the specular reflexion of the sun by the wavy sea surface. Common atmospheric correction algorithms are not designed to work in these observation conditions, reducing the spatial coverage at such latitudes by nearly a half. We describe an original atmospheric correction algorithm, named POLYMER, designed to recover ocean color parameters in the whole sun glint pattern. It has been applied to MERIS data, and validated against in-situ data from SIMBADA. The increase of useful coverage of MERIS measurements for ocean color is major, and the accuracy of the retrieved parameters is not significantly reduced in the presence of high sunglint, while, outside the sunglint area, it remains about the same as by using the standard algorithm.

OCIS codes: (010.0010) Atmospheric and oceanic optics; (280.4788) Optical sensing and sensors; (010.1285) Atmospheric correction.

References and links

1. H. Gordon, "Removal of atmospheric effects from satellite imagery of the oceans." Appl. Opt., 17: 1631-1636 (1978).
2. H. R. Gordon and D. K. Clark, "Clear water radiances for atmospheric correction of Coastal Zone Color Scanner imagery." Applied Optics, 20, 4175-4180 (1981).
3. H. R. Gordon, "Atmospheric correction of ocean color imagery in the Earth Observing System era." J. Geophys. Res., 102, D14, 17,081-17,106. (1997).
4. H. Gordon and M. Wang, "Retrieval of water-leaving radiance and aerosol optical thickness over the oceans with SeaWiFS: A preliminary algorithm." Appl. Opt., 33: 443-452 (1994).
5. D. Antoine and A. Morel, "A multiple scattering algorithm for atmospheric correction of remotely sensed ocean colour (MERIS instrument): principle and implementation for atmospheres carrying various aerosols including absorbing ones." Int. J. Remote. Sensing, 20, 9, 1875-1916 (1999).
6. M. Wang and S. W. Bailey, "Correction of sun glint contamination on the SeaWiFS ocean and atmosphere products." Appl. Opt., 40, 4790-4798 (2001).
7. M. Wang, "Remote sensing of the ocean contributions from ultraviolet to near-infrared using the shortwave infrared bands: simulations." Appl. Opt. 46, 1535-1547 (2007).
8. H. R. Gordon, T. Du, and T. Zhang, "Remote sensing of ocean color and aerosol properties: resolving the issue of aerosol absorption," Appl. Opt. **36**, 8670–8684 (1997).
9. C. Moulin, H. R. Gordon, R. M. Chomko, V. F. Banzon, and R. H. Evans, "Atmospheric correction of ocean color imagery through thick layers of Saharan dust," Geophysical Research Letters **28**, 5–8 (2001).
10. R. M. Chomko, H. R. Gordon, S. Maritorena, and D. A. Siegel, "Simultaneous retrieval of oceanic and atmospheric parameters for ocean color imagery by spectral optimization: a validation," Remote Sensing of Environment **84**, 208 – 220 (2003).
11. C. P. Kuchinke, H. R. Gordon, and B. A. Franz, "Spectral optimization for constituent retrieval in Case 2 waters I: Implementation and performance," Remote Sensing of Environment **113**, 571 – 587 (2009).
12. P. Shanmugam and Y.-H. Ahn, "New atmospheric correction technique to retrieve the ocean colour from seawifs imagery in complex coastal waters," Journal of Optics A: Pure and Applied Optics **9**, 511 (2007).

13. H. Schiller and R. Doerffer, "Neural network for emulation of an inverse model operational derivation of Case II water properties from MERIS data," International Journal of Remote Sensing, Volume 20, Issue 9, pages 1735 - 1746 (1999).
14. C. Cox and W. Munk, "Measurement of the roughness of the sea surface from photographs of the suns glitter," J. Opt. Soc. Am., 44, 11, 838-850 (1954).
15. J. Lenoble, M. Herman, J. Deuze, B. Lafrance, R. Santer, and D. Tanre, "A successive order of scattering code for solving the vector equation of transfer in the earths atmosphere with aerosols," Journal of Quantitative Spectroscopy and Radiative Transfer 107, 479507 (2007).
16. L. D'Alba and P. Colagrande, "MERIS smile effect characterization and correction," Tech. rep., ESA (2005).
17. A. Morel, "Optical modeling of the upper ocean in relation to its biogenous matter content (case I waters)," J. Geophys. Res., 93, 10749-10768 (1988).
18. A. Morel and S. Maritorena, "Bio-optical properties of oceanic waters : a reappraisal," J. Geophys. Res., 106(C4) : 7163-7180. (2001).
19. A. Morel, B. Gentili, H. Claustre, M. Babin, A. Bricaud, J. Ras, and F. Tieche, "Optical properties of the "clearest" natural waters," Limnol. Oceanogr. 52, 217-229 (2007).
20. H. Buiteveld, J. H. Hakvoort, and M. Donze, "Optical properties of pure water," in "Society of Photo-Optical Instrumentation Engineers (SPIE) Conference Series," , vol. 2258, J. S. Jaffe, ed. (1994), vol. 2258, pp. 174–183.
21. A. Morel and B. Gentili, "Diffuse reflectance of oceanic waters. II Bidirectional aspects," Appl. Opt. **32**, 6864–6879 (1993).
22. H. Loisel and A. Morel, "Light scattering and chlorophyll concentration in case 1 waters: a re-examination." Limnology and Oceanography. 43: 847-857. (1998).
23. K. G. Ruddick, V. D. Cauver, and Y. J. Park, "Seaborne measurements of near-infrared water leaving reflectance: the similarity spectrum for turbid waters." Limnol. Oceanogr., 51(2), 1167-1179 (2006).
24. J. Nelder and R. Mead, "A Simplex Method for Function Minimization," Computer Journal, vol 7, pp 308-313 (1965).
25. E. P. Shettle and R. W. Fenn, "Models for the aerosols of the lower atmosphere and the effects of humidity variations on their optical properties," AFGL-TR-79-0214, No 676 (1979).
26. C. Brockmann, "Limitations of the application of the MERIS atmospheric correction," in "Meeting on MERIS and AATSR Calibration and Geophysical Validation (MAVT-2006)," (2006).
27. G. Bécu, "Contribution à la vérification des observations spatiales de la couleur de l'océan à l'aide du réseau de radiomtres optiques SIMBADA," Ph.D. thesis, Laboratoire d'Optique Atmosphérique (2004).
28. K. Barker, C. Mazeran, C. Lerebourg, M. Bouvet, D. Antoine, M. Ondrusek, G. Zibordi, and S. Lavender, "MERMAID: The MEris MAtchup In-situ Database," MERIS and (A)ATSR Workshop, Frascati (2008).
29. A. Morel and D. Antoine, "Pigment index retrieval in case 1 waters, ATBD 2.7 MERIS," Tech. rep., Laboratoire d'Océanographie de Villefranche (2007).
30. D. Antoine, F. d'Ortenzio, S. B. Hooker, G. Bécu, B. Gentili, D. Tailliez, and A. J. Scott, "Assessment of uncertainty in the ocean reflectance determined by three satellite ocean color sensors (MERIS, SeaWiFS and MODIS-A) at an offshore site in the Mediterranean Sea (BOUSSOLE project)," Journal of Geophysical Research (Oceans), 113, C07013 (2008).

1. Introduction

It is common to affirm that atmospheric correction is paramount for the estimate of ocean color, the spectrum of marine reflectance, from space. The large atmospheric scattering dominates the weak contribution from the ocean scattering, by typically ten times. Atmospheric correction methods have been studied and have evolved from the early times of the Coastal Zone Color Scanner (CZCS) experiment [1, 2] to the so-called Earth Observing System (EOS) era [3]. The more recent experiments, Sea-viewing Wide Field-of-view Sensor (SeaWiFS) [4], the Moderate Resolution Imaging Spectroradiometer (MODIS), the Medium Resolution Imaging Spectrometer Instrument (MERIS) [5], POLDER (POLarization and Directionality of the Earth's Reflectances), all have spectral bands in the near infrared (NIR) that allow to accurately determine the aerosol scattering properties for atmospheric correction, assuming a black ocean at these wavelengths. Based on common basis of the use of NIR bands, many atmospheric correction algorithms have been developed and successfully tested to derive ocean parameters, namely marine reflectance and chlorophyll concentration.

The early experiments from CZCS, to SeaWiFS, and to POLDER, had a tilting capacity to avoid observation in the sun glint pattern, direct solar radiation reflected by the wavy sea sur-

face. More recently MODIS or MERIS have a fixed field of view pointing at nadir for practical reasons, with the downside of observing a large and intense glitter pattern at subtropical latitudes. Traditional atmospheric correction methods then fail to retrieve the marine parameters, at the expense of degrading the spatial coverage of the useful ocean color product.

The challenge to correct for both atmospheric scattering and glitter is formidable due to the difficulty to determine their parameters from a few NIR spectral bands. In the sunglint area, one has to determine three parameters to make the atmospheric correction, the aerosol optical thickness and its spectral behaviour, and also the wind speed at the sea surface for glitter prediction. Previous attempts have been made to correct for a small glint contamination in SeaWiFS data [6], using wind speed predictions. The use of additional bands in the short wave infrared has also been investigated [7]. Some alternative approaches have been proposed, based on the use of a wider range of spectral bands into spectral optimization methods: some of these approaches are targeted on absorbing aerosols [8, 9, 10], and case 2 waters [11, 12]. Doerffer *et al.* [13] have also proposed a method based on neural networks, and have applied this method both on case 2 waters and sun-glint contaminated observations. All these methods share the common point that the atmospheric and oceanic parameters are retrieved simultaneously.

In the present study we have investigated an other alternative candidate algorithm named POLYMER (POLYnomial based algorithm applied to MERIS). This algorithm is also based on spectral optimization, but with a different approach. It is applicable in the whole glitter pattern, and makes use of the whole spectral range, from blue to NIR bands. Emphasis will be put to make the application of the POLYMER algorithm to the processing of MERIS data.

2. Description of the algorithm

In the atmospheric correction algorithms currently used to process MERIS and MODIS data from Level 1 to Level 2 to obtain the ocean products [4, 5], the variable signal of the aerosols is estimated at near infrared bands and extrapolated in the green and blue bands. While weak sun glint contaminations can be estimated and corrected for, up to reflectances in the order of 0.5% [6], this method does not work when the observation is dominated by the sun glint. In this case, the spectral contamination of the sun glint can not be estimated with sufficient accuracy by using only near infrared bands, because of the high variability of the sun glint, but also its couplings with the aerosol and Rayleigh scatterings. Therefore, it seems necessary to use a wider range of spectral bands to estimate the atmospheric and sun glint correction.

The principle of the POLYMER algorithm is a spectral matching method: it is based on (1) a polynomial used to model the spectral reflectance of the atmosphere and sun glint, (2) a water reflectance model and (3) the use of all available spectral bands in the visible. In this part, we describe the models and the method used in the POLYMER atmospheric correction scheme.

2.1. Decomposition of the top of atmosphere signal

The radiance L_{TOA} measured at wavelength λ at the top of the atmosphere (TOA) with a solar zenith angle θ_s, is converted to reflectances ρ_{TOA} by normalization to extraterrestrial solar irradiance F_0:

$$\rho_{\mathrm{TOA}}(\lambda) = \frac{\pi L_{\mathrm{TOA}}(\lambda)}{\cos(\theta_s) F_0(\lambda)} \tag{1}$$

This reflectance can be decomposed as follows:

$$\rho_{\mathrm{TOA}}(\lambda) = t_{\mathrm{oz}}(\lambda) \cdot \left[\rho_{\mathrm{mol}}(\lambda) + T(\lambda)\rho_{\mathrm{gli}} + \rho_{\mathrm{aer}}(\lambda) + \rho_{\mathrm{coupl}}(\lambda) + t(\lambda)\rho_w^+(\lambda)\right] \tag{2}$$

In this decomposition, $t_{\mathrm{oz}}(\lambda)$ is the transmittance of the ozone, $\rho_{\mathrm{mol}}(\lambda)$ is the Rayleigh scattering, ρ_{gli} is the (non-spectral) sun glint reflectance transmitted by the direct transmission

factor $T(\lambda)$, $\rho_{\text{aer}}(\lambda)$ is the reflectance of the aerosols (which are considered non-absorbing), $\rho_{\text{coupl}}(\lambda)$ accounts for the various coupling terms between the sun glint, the molecules and the aerosols, $t(\lambda)$ is the total (direct and diffuse) transmission for atmospheric scattering and $\rho_w^+(\lambda)$ is the water reflectance above the water-air interface.

The first step is to correct the measured signal for the effects that can be accurately predicted: the ozone transmission $t_{\text{oz}}(\lambda, U_{\text{oz}})$, depending on the total ozone concentration U_{oz} obtained from ECMWF data (European Centre for Medium-Range Weather Forecasts), and the Rayleigh scattering, depending on the observation geometry and atmospheric pressure at sea level P_0. Also, an initial correction for the sun glint is performed: it is estimated from the wind speed ECMWF data using the sea surface roughness model by Cox and Munk [14], without including wind direction. The term associated with this initial correction is given by $\rho_{\text{mol+gli}}(\lambda, V_{\text{wind}})$, which includes Rayleigh scattering, the sun glint and the coupling between Rayleigh scattering and sun glint. It is calculated with the Successive Order of Scattering radiative transfer code (SOS, [15]) and stored in look-up to save computation time. This term at wavelength λ depends on the following parameters: the sun and sensor zenith angles, the relative azimuth angle, the surface pressure (these parameters are omitted for clarity) and the wind speed. Thus, the initial correction writes:

$$\rho'(\lambda) = \frac{\rho_{\text{TOA}}(\lambda)}{t_{\text{oz}}(\lambda)} - \rho_{\text{mol+gli}}(\lambda, V_{\text{wind}}) \tag{3}$$

In this initial correction, the wind speed at each pixel is not known accurately; consequently, there can be a large difference (several percents) between the simulated and actual sun glint. Therefore, a misestimation of the wind speed will lead to a misestimation of $\rho'(\lambda)$, and can possibly lead to negative values of $\rho'(\lambda)$. This is not a problem since only the spectral shape of this term is important in the present atmospheric correction process, rather than its absolute values. The choice of still doing a rough initial correction for the sun-glint is made to remove a significant portion of the sun glint, thus reducing the amplitude of the remaining signal to be corrected for. To account for the inaccuracy of this initial correction, a residue $\Delta\rho_{\text{gli}}(\lambda)$ of sun glint and its coupling with Rayleigh scattering is introduced:

$$\rho_{\text{mol}}(\lambda) + T(\lambda)\rho_{\text{gli}} = \rho_{\text{mol+gli}}(\lambda, V_{\text{wind}}) + \Delta\rho_{\text{gli}}(\lambda) \tag{4}$$

Thus, $\rho'(\lambda)$ can be written as:

$$\rho'(\lambda) = \rho_{\text{ag}}(\lambda) + t(\lambda)\rho_w^+(\lambda) \tag{5}$$

where $\rho_{\text{ag}}(\lambda)$ represents the residue of sun-glint, the aerosol scattering and the coupling terms:

$$\rho_{\text{ag}}(\lambda) = \Delta\rho_{\text{gli}}(\lambda) + \rho_{\text{aer}}(\lambda) + \rho_{\text{coupl}}(\lambda) \tag{6}$$

Like $\rho_{\text{mol+gli}}$, the term $t(\lambda)$ is pre-calculated with the SOS code and stored in look-up tables. In this case, the assumption is that the transmission of the aerosols is negligible, which is valid in most cases — when the aerosols are not absorbing. Thus, it is approximated as the transmission factor of an atmosphere containing only molecules, and is calculated under the same conditions as $\rho_{\text{mol+gli}}$. It depends on the following parameters: the sun and sensor zenith angles, the surface pressure and the wind speed.

The objective of the algorithm will be to decompose $\rho'(\lambda)$ into the ocean water scattering $\rho_w^+(\lambda)$ and the signal scattered by the atmosphere and the residual sun glint $\rho_{\text{ag}}(\lambda)$. This decomposition is based on the models described herein.

2.2. *Atmospheric model*

If we assume that the water reflectance spectrum is known, the reflectance of the residual sun glint, aerosols and couplings $\rho_{\mathrm{ag}}(\lambda)$ is numerically given by $\rho'(\lambda) - t(\lambda)\rho_w^+(\lambda)$. The basic principle of the POLYMER algorithm is to model this atmosphere contribution and the residual sun glint as a polynomial with three terms:

$$\rho_{\mathrm{ag}}(\lambda) \approx T_0(\lambda)c_0 + c_1\lambda^{-1} + c_2\lambda^{-4} \tag{7}$$

By introducing this model, we do not try to model each individual component among the glitter, the aerosols and the couplings. Instead, we choose to model the various terms of $\rho_{\mathrm{ag}}(\lambda)$, as described in Eq. 6, as a whole, by the previous polynomial. The coefficients c_0, c_1 and c_2 are estimated by least square fitting of the observation ; the method will be detailed in part 2.4.

The motivation for this model is that we expect the signal $\rho_{\mathrm{ag}}(\lambda)$ to contain the following spectral components:

- spectrally flat components: the residual sun glint, but also the cloud reflectance and the large particle scattering (aerosol coarse mode: maritime aerosols, cloud droplets, dust). A transmission factor $T_0(\lambda)$ is applied to this term, and accounts for the beam attenuation due to Rayleigh scattering (the transmission by aerosols is neglected). In presence of sun glint (a specular target), this transmission is the direct transmission, which is given by:

  $$T_0^{\mathrm{dir}}(\lambda) = \exp\left[-\tau_m(\lambda) \times (\frac{1}{\mu_s} + \frac{1}{\mu_v})\right]$$

  In this expression, μ_s and μ_v are the cosines of the solar and view zenith angles, and the Rayleigh optical thickness $\tau_m(\lambda) \approx 0.00877\lambda^{-4.05}$, with λ in nm. In presence of a lambertian target (cloud droplets, maritime aerosols), the diffuse transmission can be approximated by:

  $$T_0^{\mathrm{dif}}(\lambda) = \exp\left[-\frac{\tau_m(\lambda)}{2} \times (\frac{1}{\mu_s} + \frac{1}{\mu_v})\right]$$

  The predicted reflectance of the sun glint (using wind data from ECMWF) is used to switch between the direct (in the sun glint, where $\rho_{\mathrm{gli}} > \rho_{\mathrm{gli,0}}$, with $\rho_{\mathrm{gli,0}} = 2\%$) and diffuse (outside sun glint, where $\rho_{\mathrm{gli}} < \rho_{\mathrm{gli,0}}$) transmission factors:

  $$T_0(\lambda) = \exp\left[-\tau_m(\lambda) \times (1 - \frac{1}{2}\exp(-\frac{\rho_{\mathrm{gli}}}{\rho_{\mathrm{gli,0}}})) \times (\frac{1}{\mu_s} + \frac{1}{\mu_v})\right]$$

- the aerosol signal, with a spectral dependency (Angstrom coefficient) in the order of -1 (aerosol fine mode),

- the couplings between flat components and the Rayleigh scattering, with a spectral dependency in the order of -4.

The actual spectral dependencies of these various components can vary, for example the aerosols Angstrom coefficient can vary from less than 0.2 to more than 1.5. Also, a transmission factor applies to the spectrally flat sun glint, and, to a lesser extent, to the scattering of semi-transparent clouds. These variations of spectral dependency will by automatically taken into account in the polynomial fitting process, leading to a balance between the three terms c_0, c_1 and c_2.

It is worthwhile to note that in this model, the wavelength λ is the central wavelength for the considered band; for MERIS, this wavelength is known to vary cross-track (this is often

referred to as the "smile effect"). This variation is larger than 1 nm at all bands, and leads to large errors in the retrieval of ocean color parameters, if not taken into account. This effect is generally corrected at level 1 by a linear interpolation technique [16]. Instead, we chose in POLYMER to keep the level 1 raw reflectances (not corrected for the smile effect), and to use for each pixel the exact central wavelength in the atmospheric correction process.

2.3. Ocean reflectance model

The bio-optical water reflectance model used in the atmospheric correction process uses two parameters: the chlorophyll concentration and the backscattering coefficient of noncovarying particles $b_{bNC}(\lambda)$; it is taken just above the surface and will be noted $\rho^{+}_{wmod}([\text{chl}], b_{bNC}, \lambda)$. The spectrum has been modelled according to Morel [17], including the updates from Morel and Maritorena [18]. Following Morel *et al.* [19], the scattering coefficient of pure water $b_w(\lambda)$ is taken from Buiteveld *et al.* [20], and multiplied by a factor 1.3 to account for the increase of scattering due to the presence of salts in the ocean water. The output of this model is the spectrum of water irradiance reflectance just beneath the surface, between 350 and 700 nm, and noted $R^{-}_{wMM}(\lambda)$. The conversion to reflectance above the surface is done by assuming that the radiance in-water is lambertian. This is a rough assumption, because angular variations in the order of 20 to 50% are expected, depending on the viewing geometry [21]. This assumption has been made to simplify the model, and it is likely that taking the bidirectional effects of water reflectance into account, will lead to a better accuracy of the retrieved parameters. The following mean transmission factor is used to convert the irradiance reflectance beneath the surface into reflectances above the surface: $\rho^{+}_{wMM}(\lambda) = 0.544 R^{-}_{wMM}(\lambda)$.

The backscattering coefficient of noncovarying particles $b_{bNC}(\lambda)$ has been added to the total backscattering coefficient. The spectral dependency for this term has been chosen to be λ^{-1}: the backscattering coefficient of phytoplankton and its covarying particles, becomes:

$$R^{-}_{wMM}(\lambda) = f\,\frac{\frac{1}{2}b_w(\lambda) + b_{bp}(\lambda) + b_{bNC}(\lambda)}{a(\lambda)} \tag{8}$$

There are several reasons for adding this variable backscattering coefficient: (1) even in case 1 waters, there is a large variability of the total backscattering coefficient around the mean b_{bp}-to-chl relationship [22]. Notably, if this variability is not taken into account, the retrieved reflectances at 510 nm are almost constant, which is anomalous, and has been verified on in-situ data (but not detailed in this paper for brevity). More generally, we have verified that there is a better fit between the reflectances estimated by POLYMER and *in-situ* data when this variable parameter is introduced. (2) Even though the algorithm is not primarily targeted at case 2 waters, the presence of the variable backscattering coefficient makes it possible to behave correctly in coastal waters. Without this coefficient, anomalous reflectances are retrieved, with values decreasing toward the coast at all bands. This term being introduced, the iterative scheme described by [18] is followed to generate the modified spectrum.

This model has also been extended from 700 nm to 900 nm, by using the similarity spectrum for turbid waters [23]: the similarity spectrum is normalized at 700 nm to ensure continuity at this wavelength:

$$\rho^{+}_{wmod}([\text{chl}], b_{bNC}, \lambda) = \begin{cases} \rho^{+}_{wMM}([\text{chl}], b_{bNC}, \lambda) & [\lambda < 700 \text{ nm}] \\ \rho^{+}_{wS}(\lambda)\rho^{+}_{wMM}([\text{chl}], b_{bNC}, 700\text{nm})/\rho^{+}_{wS}(700\text{nm}) & [\lambda \geq 700 \text{ nm}] \end{cases} \tag{9}$$

The resulting spectra are presented on Figs. 1a and 1b. Fig. 1a shows the spectrum of case 1 waters, and its extension up to 900 nm using the similarity spectrum (the two spectra overlap

between 650 and 700 nm). In the range 700 to 900 nm, a very similar spectrum is obtained when using the reciprocal of the pure water absorption coefficient ($1/a_w(\lambda)$), as demonstrated in [23]. Fig. 1b shows the modeled spectra for two chlorophyll concentrations and three values of b_{bNC}: the latter parameter introduces an offset on the spectrum, but does not change significantly its shape.

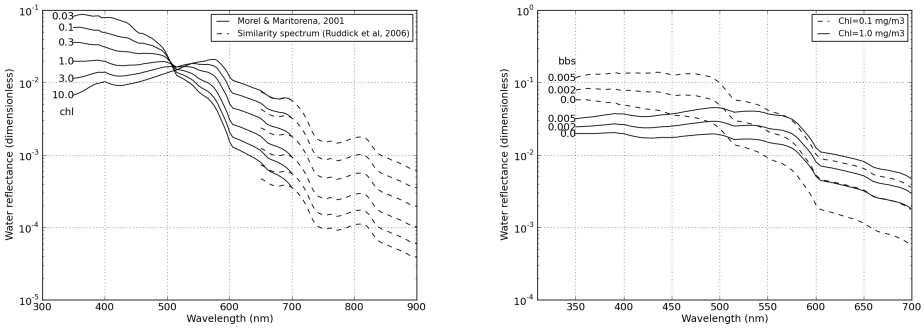

(a) (b)

Fig. 1. Examples of spectra for the model of water reflectances used in this study. It is based on two parameters: the chlorophyll concentration (chl) and the backscattering coefficient of suspended matter (b_{bNC}). On Fig. 1a, b_{bNC} is set to zero, and thus corresponds between 350 and 700 nm to the model by [18] (solid curve). It is extended from 700 to 900 nm using the similarity spectrum for turbid waters [23] (dashed curves). Fig. 1b shows how the spectrum varies with the parameter b_{bNC}, for two chlorophyll concentration.

2.4. Spectral matching

The goal of the POLYMER algorithm is to use the two models previously described, to separate the signal $\rho_{ag}(\lambda)$, from the signal scattered by the sea water. The whole range of available spectral bands can be used for this process. This technique of spectral matching consists in optimizing the parameters of the atmospheric model (c_0, c_1 and c_2) and the parameters of the ocean water reflectance model ([chl] and b_{bNC}), in order to obtain the best spectral fit of $\rho'(\lambda)$. In this scheme, a subset of N bands in all available spectral bands is used. It is theoretically possible to use any subset of the available bands, with a minimum of $N = 5$ bands corresponding to the number of parameters. MERIS instrument has 15 bands, and we have discarded 5 of them: 681 (chlorophyll fluorescence peak), 709 (imprecise correction for water vapour absorption), 760 (oxygen absorption band), 885 and 900 nm (reduced signal-to-noise). Therefore the $N = 10$ remaining bands previously mentioned in part 2.2 are used.

The 10-based logarithm of the chlorophyll concentration will be noted as logC. The scheme is the following:

- Consider the following cost function $f : (\mathrm{logC}_i, b_{bNC,i}) \rightarrow \varepsilon_i$:
    1. For the current values of logC_i and $b_{bNC,i}$, and for each wavelength λ among the N selected bands, calculate the water reflectance spectrum $\rho^+_{w\mathrm{mod}}([\mathrm{chl}]_i, b_{bNC,i}, \lambda)$ from the model described in section 2.3
    2. Calculate the values of c_0, c_1 and c_2 obtained by the polynomial fit for all wavelengths λ:

$$T_0(\lambda)c_0 + c_1\lambda^{-1} + c_2\lambda^{-4} \approx \rho'(\lambda) - t(\lambda)\rho^+_{wmod}([\mathrm{chl}]_i, b_{bNC,i}, \lambda)$$

3. Calculate the mean square error ε_i of the previous fit:

$$\varepsilon_i = \frac{1}{N}\sum_{\lambda_j}\left\{T_0(\lambda)c_0 + c_1\lambda_j^{-1} + c_2\lambda_j^{-4} - \left[\rho'(\lambda_j) - t(\lambda_j)\rho^+_{wmod}([\text{chl}]_i, b_{bNC,i}, \lambda_j)\right]\right\}^2$$

This function $f : (\log C_i, b_{bNC,i}) \rightarrow \varepsilon_i$ represents the mean square error between the atmosphere and residual sun glint reflectances and its polynomial fit. The objective is then to minimize f with respect to the parameters logC and b_{bNC}.

- The final values of logC and b_{bNC} are obtained by a n-dimensional iterative minimization technique of the cost function f, using a simplex method [24]. This technique consists in constructing successive polygons with n+1 vertices, called simplexes, by replacing at each iteration the vertex with the highest value, in order to converge toward a local minimum of the function f. In our case, n=2 and the simplexes are triangles. The first iteration simplex is defined by initial values $\log C_0 = 0$ and $b_{bNC,0} = 0$, and initial steps $\Delta\log C_0 = 0.05$ and $\Delta b_{bNC,0} = 5\times10^{-4}$. The stopping criterion of this scheme is a threshold on the size of the simplex: this size is defined as the average distance between the center of the simplex and its vertices. The value of this threshold has been set to 0.005.

When the stopping criterion is achieved, we obtain the final values of the parameters c_0, c_1 and c_2, [chl] and b_{bNC}. With the final values of the coefficients c_i, the spectrum of water reflectances $\rho^+_w(\lambda)$ is given by the following relationship:

$$\rho^+_w(\lambda) = \frac{\rho'(\lambda) - (T_0(\lambda)c_0 + c_1\lambda^{-1} + c_2\lambda^{-4})}{t(\lambda)} \tag{10}$$

2.5. Application to synthetic data

To estimate the theoretical accuracy and the characteristics of this algorithm, we have applied it to a synthetic dataset. This dataset has been generated by the SOS radiative transfer code, with ocean reflectances obtained by the model previously described. Only case 1 waters have been simulated ($b_{bNC} = 0$), and the chlorophyll concentrations range is 0.03 to 10 mg/m3 (12 values equally spaced in logarithmic scale). For each chlorophyll concentration, a combination of various atmospheric conditions have been simulated:

- Various observation geometries, including various sun glint conditions: 9 values of equally spaced relative azimuth angle ranging from 0 to 180°, two sun zenith angles (17.6°and 36.2°), and two view zenith angles (6.5°and 25.0°)
- Various aerosol optical thicknesses at 865 nm: 0., 0.01, 0.02, 0.05, 0.1, 0.2 and 0.4
- 12 aerosol models by Shettle and Fenn [25]: M98, M95, M90, M80, C90, C80, C70, T99, T98, T90, T80, T70

The wind speed is set to 5 m/s, which determines the sun glint intensity from the Cox and Munk model. For these conditions, three cases are considered: (1) a "mixed" case: $\rho_{\text{gli}} < 10\%$, (2) a "no aerosol" case: $\tau_{\text{aer}} = 0$, no limit on ρ_{gli} and (3) a "no glint" case: $\rho_{\text{gli}} < 1\%$.

Then, noise has been optionally added to the synthetic values of TOA reflectances, with signal to noise ratios (SNR) typical of future Sentinel-3 instrument. The SNR values are wavelength dependent and also depend on the TOA radiances: the order of magnitude of SNR is about 700 in blue bands to about 400 in the NIR. The resulting sets of TOA reflectances have been processed with POLYMER, and the simulated values are compared to the retrieved values. In few particular condition, the algorithm is unstable: this condition is the lowest chlorophyll

concentration (0.03 mg/m3) and moderate to high glint condition (125 items out of 31248 in the "mixed" case). The algorithm then retrieves high chlorophyll concentration and negative values of b_{bNC}, which is not physical; these cases are flagged out. However, such instabilities have not been observed in real images, and these cases are removed from the comparison.

In this processing, the wind speed used for the initial molecular and sun glint correction is 7 m/s: this value is purposely different from the value of 5 m/s used in the simulation, because the wind speed should not be considered to be known exactly. We have verified that if we use a wind speed of 5 m/s for this initial correction, and in absence of aerosol and additional noise, the simulation conditions are retrieved very well.

The comparison between synthetic and retrieved data is presented on Fig. 2. These figures include noise addition. For the "mixed" case (first column), we can see that the chlorophyll concentration is very well retrieved ($R^2 = 0.995$). The water reflectances at 443 and 560 nm are slightly biased low, but are still very well correlated with the simulations. The figures in the second column show the dependency between the error on each parameter and the sun glint intensity ("no aerosol" dataset). We can see that the retrieval of all parameters is almost independent of the sun glint intensity; the scatter increases only slightly with ρ_{gli} and no significant bias is observed. In particular, the water reflectances are retrieved with a bias lower than 1% and a RMSE lower than 5%, even in presence of a sun glint reflectance as high as 14%. The figures on the third column show the dependency between the error on each parameter and the aerosol optical thickness ("no glint" dataset). In this case, we can see larger errors and a negative bias on the water reflectances, which increase with the aerosol load: large aerosol plumes with optical thicknesses at 865 nm in the order or greater than 0.4 may be degraded. However, the error on the chlorophyll concentration is lower than the error on the reflectances. More generally, the retrieval of chlorophyll concentration is more robust than the retrieval of water reflectances, which is also the case for traditional atmospheric correction methods.

Figs. 3a and 3b summarize the relative bias and RMSE of the comparisons between synthetic and retrieved reflectances at each wavelength. We can see that the retrieved values are slightly low biased, (between 2 and 4% bias on the water reflectances). The effect of the noise on the bias is negligible. We also notice that the RMSE increase with the added noise is very moderate: the RMSE increases by less than 2% at all bands except 670 nm (where the reflectances are very small), which is in complete agreement with typical requirements on ocean color products. The RMSE of the water reflectances due to the method is in the order of 6-8% for the "mixed" case. It is noteworthy that the selected dataset ("mixed" case) is not intended to be representative of real data, and does certainly exaggerate the frequency of "difficult cases" (especially, the presence of aerosols).

This application to synthetic data has permitted to quantify the residue of atmospheric correction, by focusing on the major unknown signals: the sun glint and the aerosol scattering. It has shown that the instrumental noise propagates very moderately from TOA to oceanic reflectances through the atmospheric correction process. Moreover, residual errors are observed even in absence of additional noise, which suggests some residual differences between the polynomial atmospheric model and the actual spectral signal. These residual errors appear to be more correlated with the presence of aerosols than with the sun glint contamination — the errors on the water reflectances are indeed very weakly correlated with intensity of the sun glint in absence of aerosols.

3. Application to MERIS data

3.1. Level 2 products

POLYMER level 2 chlorophyll concentration parameters are presented together with MERIS MEGS 7.4 "algal 1" parameters. Figs. 4a to 4d present the results on a sun-glint contaminated

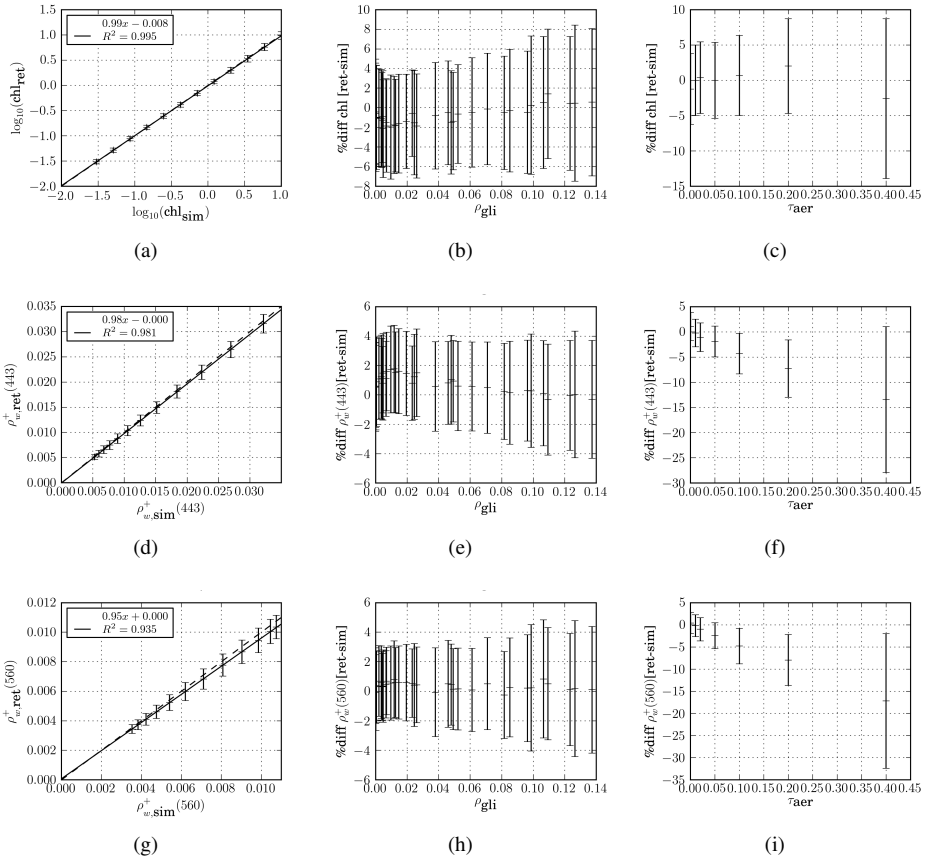

Fig. 2. Plots for the comparison between the simulated parameters (synthetic dataset, indicated by subscript "sim"), and the parameters retrieved by POLYMER (indicated by subscript "ret"). In these figures, noise has been added to TOA reflectances according to typical Sentinel-3 SNR. Each row corresponds to the following parameters: chlorophyll concentration, water reflectance at 443 nm and 560 nm. The first columns (Figs. (a), (d) and (g)) shows the regression between the synthetic and retrieved parameters, for the "mixed" case. The second columns (Figs. (b), (e) and (h)) shows the relative percent difference, between the retrieved and synthetic values ($\frac{\text{ret-sim}}{\text{sim}}$), as a function of the sun glint reflectance; emphasis is put on the sun glint correction by using the case "no aerosol". The difference between $\log_{10}(\text{chl}_{\text{ret}})$ and $\log_{10}(\text{chl}_{\text{sim}})$ is multiplied by $\ln(10)$ to convert to relative percent difference of the chlorophyll concentration ($\frac{\Delta\text{chl}}{\text{chl}} \approx \ln(10)\Delta\log_{10}(\text{chl})$). The third columns (Figs. (c), (f) and (i)) shows the relative percent difference, between the retrieved and synthetic values, as a function of the aerosol optical thickness at 865 nm; emphasis is put on the aerosol correction by using the case "no glint".

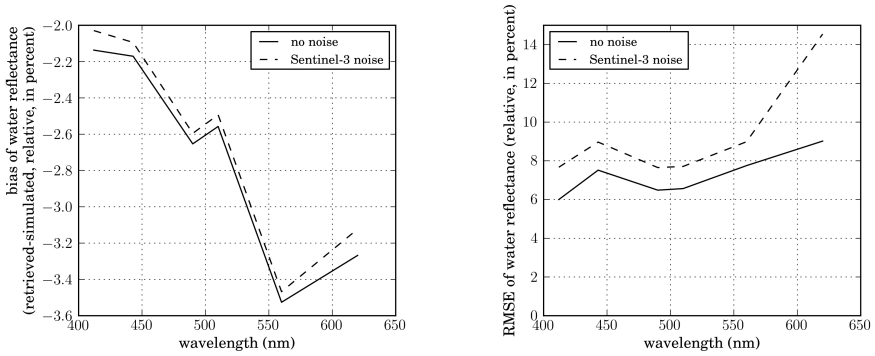

Fig. 3. Summary of the relative biases (a) and RMSE (b) of the comparison between synthetic and retrieved water reflectances at each wavelength, for the "mixed"case, with and without noise added to TOA reflectances.

MERIS scene in Mediterranean Sea. The sun glint reflectance is in the order of 10%. Figures 4a and 4b show the chlorophyll concentration parameter obtained by MEGS 7.4 processor (the pixels flagged by "PCD_15" MERIS flag are removed, which is commonly done to remove invalid chlorophyll concentration results) and by the POLYMER algorithm. We can see that the two chlorophyll parameters are slightly biased in the low chlorophyll concentration range, but otherwise in good agreement; the chlorophyll field is consistently retrieved by POLYMER, but the standard algorithm retrieves invalid values over the sun glint pattern. The same observations applies to the $\rho_w^+(560)$ parameter (Figs. 4c and 4d, where pixels flagged by "PCD_1_13" MERIS flag are removed (which is commonly done to remove invalid reflectance values); for this parameter we notice that invalid values are also retrieved in coastal areas, as can be seen for example around Majorca. As for the chlorophyll concentration, POLYMER also retrieves slightly lower water reflectances at 560 nm than the standard algorithm.

On Figs. 5a to 5f, we can see a MERIS scene over Sea of Japan / East Sea. This scene is not contaminated by sun glint, but by a large aerosol plume, with an optical thickness greater than 0.5 (Figs. 5a and 5d). We can see that the standard atmospheric correction algorithm fails in this aerosol plume (Fig. 5b) but the POLYMER algorithm succeeds in recovering a consistent chlorophyll concentration field (Fig. 5c). The figures 5e and 5f show the retrieved values of the atmospheric parameters c_0 and c_1. We can see that the parameter c_0, which corresponds to flat spectral components, increases over semi-transparent clouds, but not over the aerosol plume. The parameter c_1 increases over the aerosol plume, where the spectral dependency is closer to λ^{-1}. Thus, the effects of the clouds and aerosols are clearly distinguished.

3.2. Level 3 products

With the possibility to retrieve ocean color products in the sun glint, a period of 3 days (the period required for MERIS to achieve a global coverage of the earth) is sufficient to obtain overlapping swaths at mid-tropical latitudes. A longer period is required to achieve satisfactory coverage with the standard atmospheric correction algorithms where the sun glint observations are not available. This is illustrated on Figs. 6 (global composite) and 7 (detail over the Arabian Sea), where composites of chlorophyll concentration over 3 days, for the MEGS product (Figs. 6a and 7a) and the POLYMER product (Figs. 6b and 7b). No obvious discontinuity between overlapping swaths, nor bias in the sun glint area can be seen in the POLYMER products.

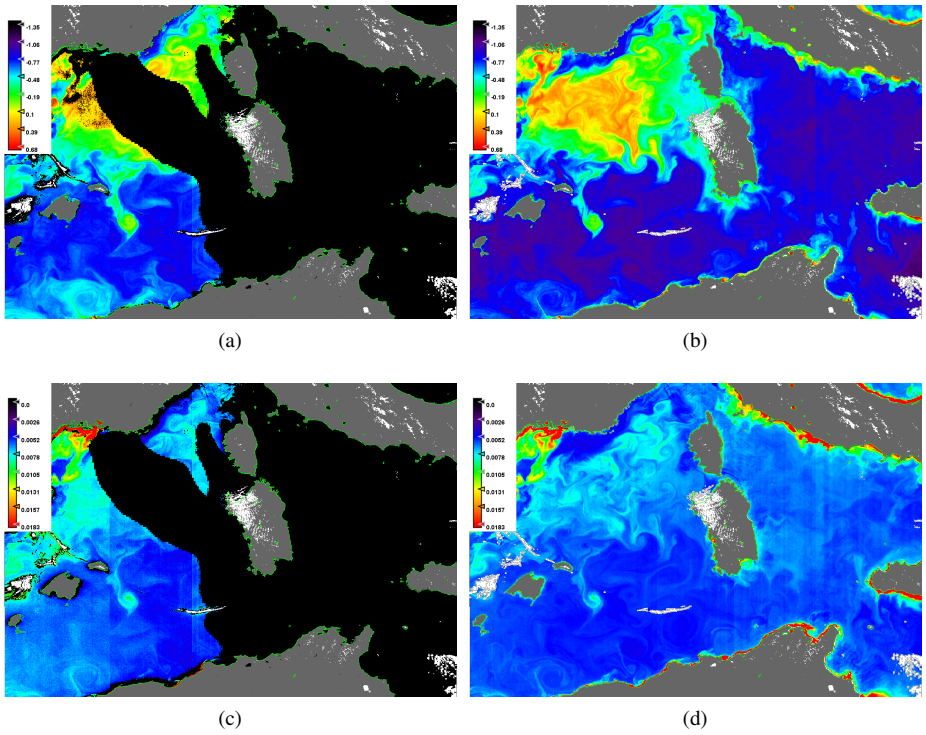

(a) (b)

(c) (d)

Fig. 4. MERIS image from Mediterranean Sea, May 7, 2005. This image is contaminated by high sun glint on the right side of the image ($\rho_{\text{gli}} \approx 10\%$). (a) Chlorophyll concentration for MEGS (”algal 1” parameter, black area is ”PCD_15”), and (b) POLYMER algorithm. The color scale represents $\log_{10}(\text{chl})$. (c) Water reflectance at 560 nm, for MEGS (black area is ”PCD_1_13”), and (b) POLYMER algorithm.

The filter applied to the level 2 products for the generation of these composites is of great importance regarding their quality and spatial coverage. For the MERIS/POLYMER composites, only a basic cloud mask (designed to avoid masking out the sun glint) has been used to filter out pixels ; for the MERIS/MEGS composite, the pixels classified as high glint, absorbing aerosols and ”PCD_1_13” are removed to obtain sufficient quality. The flag ”PCD_1_13” (processing MEGS 7.4) is raised when at least one water reflectance is negative, which happens frequently in presence of semi-transparent clouds, resulting in degraded estimation [26].

The increase of global spatial coverage is detailed in table 1. This table gives the percentage of all the non-cloudy pixels from the 43 orbits used in the global 3 days composite of Figs. 6 and 7, for the three different sun glint flags (”no glint”, ”medium glint” and ”high glint”). The three columns represent respectively all the (non-cloudy ocean) pixels, the pixels where the quality flag ”PCD_1_13” is not raised, and the valid POLYMER pixels. We can see that about half of the pixels are not contaminated by sun glint, and about a third are highly contaminated; for nearly all the pixels, the POLYMER processing is valid (the output values are within a range considered as ”valid”: chlorophyll concentration between 0.01 and 100, and $b_{bNC}(550)$ between -5×10^{-3} and 0.1). If we decide to flag out the pixels ”HIGH GLINT” and ”PCD_1_13” in the MEGS product, which seems reasonable regarding the quality of the MEGS products for these flags, we can see that this leaves 31% of the pixels; thus, the increase of spatial coverage by using the POLYMER algorithm is roughly a factor 3.

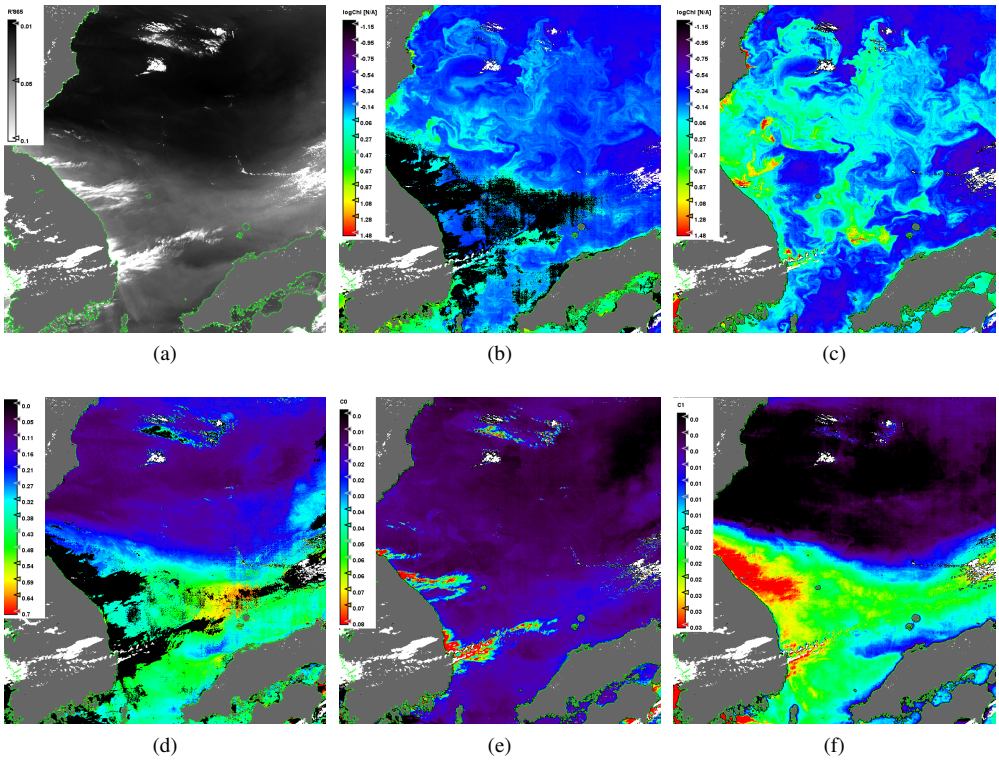

Fig. 5. MERIS image from Sea of Japan / East Sea, 2004-03-13. (a) An aerosol event can be seen on the parameter $\rho_{\hat{865}}$ and (d) the aerosol optical thickness at 865 nm from MEGS processing. (b) and (c) show the chlorophyll concentration estimated respectively by the MEGS and POLYMER algorithms. (e) and (f) show the parameters c_0 (flat spectral dependency) and c_1 (spectral dependency in λ^{-1}) estimated by POLYMER.

The details of the distribution of the flags at level 2 is presented on table 1; however the increase of coverage on global composites is significantly smaller, because of the overlap between adjacent POLYMER swaths. Such overlaps will lead to areas observed several times over the considered period of 3 days, without increasing the coverage of the composite. Thus, the surface of the oceans covered by the composites of Figs. 6a and 6b, for a period of 3 days, is respectively 30.1% (MERIS/MEGS 7.4) and 53.7% (MERIS/POLYMER).

4. Validation with SIMBADA *in situ* data

This part presents a validation of POLYMER level 2 water reflectances against *in situ* data from the optical radiometer SIMBADA (Satellite Intercomparison for Marine Biology and Aerosol Determination - Advanced version) [27]. The MERMAID database [28] has been used to obtain the SIMBADA *in situ* data together with the MERIS level 1 and level 2 match-ups.

4.1. Data and method

The SIMBADA radiometer provides estimations of water reflectance at the following MERIS bands: 412, 443, 490, 510, 560 and 620 nm. At these wavelengths, we consider the following parameters: the water reflectance from POLYMER algorithm $\rho^{+}_{w,\mathrm{POLYMER}}$, the water reflectance

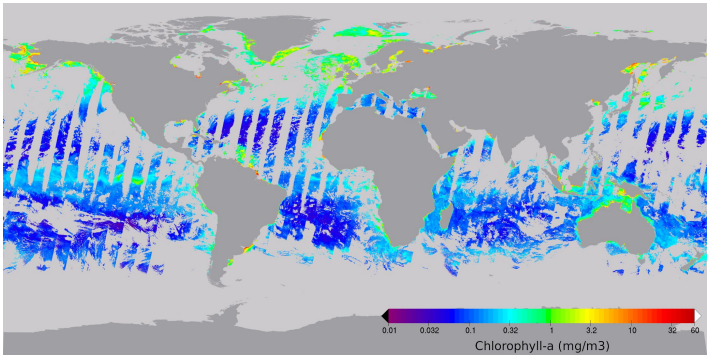

(a)

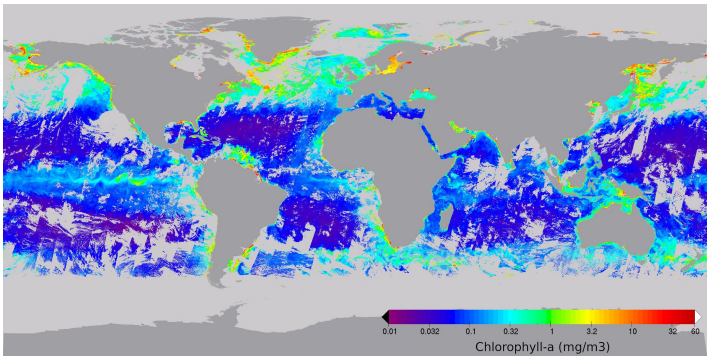

(b)

Fig. 6. Global 3 days composites of the chlorophyll concentration parameter, June 3 to 5, 2003: (a) from MERIS/MEGS 7.4 products (where the flags ”high glint”, ”PCD_1_13” and ”absorbing aerosols” have been applied to filter the pixels) and (b) from MERIS/POLYMER products.

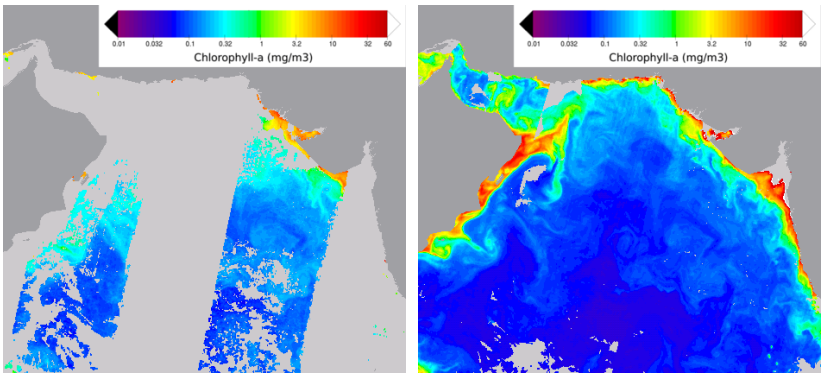

(a) (b)

Fig. 7. Detail of Figs. 6a and 6b over the Arabian Sea: (a) MERIS/MEGS 7.4 and (b) MERIS/POLYMER.

	All pixels	Pixels without "PCD_1_13"	POLYMER valid pixels
NO GLINT	52.7%	22.4%	52.3%
MEDIUM GLINT	19.0%	8.6%	18.9%
HIGH GLINT	28.3%	0.0%	28.3%
Total	100.0%	31.0%	99.5%

Table 1. Distribution of all the "non-cloudy" level 2 pixels between the MERIS level 2 sun glint flags, for the 43 orbits used to generate the global 3 days composite presented on Fig. 6. The three columns represent respectively the total number of pixels, the pixels not flagged by "PCD_1_13", and the valid POLYMER pixels. The use of the "PCD_1_13" flag to invalid some of the data from standard processing, has been shown to improve the accuracy of the remaining ones.

from official MERIS level 2 processor (MEGS 7.4) $\rho^{+}_{wn,\mathrm{MEGS}}$, the water reflectance from SIMBADA $\rho^{+}_{wn,\mathrm{INSITU}}$. The parameters $\rho^{+}_{wn,\mathrm{MEGS}}$ and $\rho^{+}_{wn,\mathrm{INSITU}}$ are normalized for ocean water bidirectional reflectance distribution function, as described in [28], but not $\rho^{+}_{w,\mathrm{POLYMER}}$. The chlorophyll concentration is also analysed: it is estimated from the water reflectances by the same bio-optical algorithm OC4Me [29].

In the comparison between the satellite water reflectance estimation and the corresponding *in situ* estimation, the matchups are split in two disjoint datasets, based on MERIS Level 2 quality flags. In all cases, "CLOUD" and "CASE2" matchups are rejected. The set 1 excludes the matchups "HIGH_GLINT" and "PCD_1_13"; it is used to validate both $\rho^{+}_{wn,\mathrm{MEGS}}$ and $\rho^{+}_{w,\mathrm{POLYMER}}$. The set 2 includes only matchups flagged as "HIGH_GLINT" or "PCD_1_13". This set is used to validate only $\rho^{+}_{w,\mathrm{POLYMER}}$.

4.2. Results

Figs. 8a to 8c illustrate the comparison between the water reflectance at 560 nm, from SIMBADA and the corresponding estimation using MERIS data. Only the central pixel of MERIS match-up is used in the comparison: macro-pixels are not used. Three sets of match-ups are considered: Figs. 8a and 8b show the results for set 1, respectively for MEGS and POLYMER, and Fig. 8c shows the result of POLYMER, for set 2, including HIGH_GLINT and PCD_1_13 points. The following statistical parameters are used: the number of points N, the slope, the correlation coefficient R^2, the accuracy (bias), and precision (root mean square error, RMSE). The reduced major axis regression line is plotted in solid. This type of regression is used because errors are known to exist also in *in-situ* data, but also to take into account the spatial and temporal discrepancies between *in-situ* and satellite measurements. On Fig. 8d, the relative percent difference between the POLYMER estimations of water reflectance at 560 nm and the corresponding SIMBADA *in-situ* measurement is plotted as a function of the sun glint reflectance ρ_{gli}.

These comparisons are repeated at other wavelengths, and also for the chlorophyll concentration. As in section 2.5, the relative percent difference in the case of chlorophyll concentration is obtained by multiplying the difference of $\log_{10}(\mathrm{chl})$ by $\ln(10)$. These results are summarized in table 2. Finally, the precision and accuracy for each dataset are shown as a function of the wavelength, on tables 9a and 9b.

The correlation between the water reflectance and the sun glint appears to be relatively weak, with a correlation coefficient R^2 lower than 8% in all cases except at 670 nm (fig. 8d and table 2). This weak residual correlation might be due to simultaneous presence of aerosols and sun

glint (the analysis of section 2.5, demonstrated the absence of correlation with the sun glint intensity, but in the absence of aerosols). The slope of the regression indicates that the water reflectance vary by about 5% at 443 nm and 21% at 560 nm, when the sun glint increases by 10% — this corresponds to a residue of 1% of the total sun glint amplitude. However, this residual correlation has to be taken with caution because of the weak correlation coefficients, and has not a major effect effect on the final precision, as can be seen on fig. 9b: between the validation without and with sun glint, the accuracy decreases by about only 15% in the blue bands.

Fig. 9b shows that the MEGS retrieval is slightly biased low in the blue, when compared to SIMBADA (about $1.5 \cdot 10^{-3}$), which has already been shown by [27]. The water reflectances retrieved by POLYMER are lower than those retrieved by MEGS in the blue, again by about $1.5 \cdot 10^{-3}$, resulting in a low bias of around $3 \cdot 10^{-2}$ in the blue. However, a validation using other *in situ* data will be useful in order to achieve a better consistency with previous studies: in particular, [30] shows an over-estimation of water reflectances by MERIS standard product in the blue.

The precision of the chlorophyll concentration parameter is better in all cases (without and with sun glint, resp. with a RMSE of 0.129 and 0.158, which correspond to relative precisions of resp. 29.7% and 36.4%) than the standard algorithm (where the RMSE is 0.207, relative precision of 47.6%). The slopes of the regressions are also significantly different between MEGS (0.78) and POLYMER (1.06 outside sun glint, 1.10 inside). This explains the visual bias between the chlorophyll concentration images shown on Figs. 4a and 4b, where the chlorophyll concentrations retrieved by POLYMER are lower than those retrieved by MEGS in the lower chlorophyll concentration range. It is worthwhile to note that set 2 includes more points than set 1; this increase in spatial coverage of a factor greater than two, is in agreement with the values given previously.

5. Conclusion

We have developed an algorithm called POLYMER to perform atmospheric correction in the sun-glint and retrieve the ocean color parameters and the spectrum of water reflectance. It is based on the idea that a flexible atmospheric model may fit the sun glint signal — even if this signal is extremely dominating and unpredictable. This algorithm uses a spectral matching method relying on two models: a simple polynomial atmospheric model representing the scattering of the atmosphere and sun-glint, and a bio-optical ocean water reflectance model. The parameters of these models are tuned in an iterative process to give the best fit of the measurements.

This algorithm has been successfully applied to MERIS imagery: the water parameters are consistently retrieved in the whole sun-glint pattern, where the specular reflection can be as bright as 20%. The comparison of the parameters retrieved by the standard algorithm MEGS 7.4 and those retrieved by POLYMER, with *in-situ* SIMBADA measurements, show a comparable accuracy of the two algorithms in absence of sun glint, and a reduction of the accuracy by about 15% in presence of sun glint. An analysis of the sources of error on the water reflectances was performed using validation with SIMBADA measurements and by applying the algorithm to simulated data. This analysis shows residual effects of the aerosol load and the sun glint intensity on the water reflectances; the decoupling between ocean and atmosphere could be improved by refining the atmospheric model. Also, this model might be extended to absorbing aerosols by adding a free absorption parameter to the atmospheric transmission factor; however in this case, it might be inevitable to compensate this additional parameter by a constraint on the other free parameters, such as neglecting the variations of the backscattering coefficient of noncovarying particles.

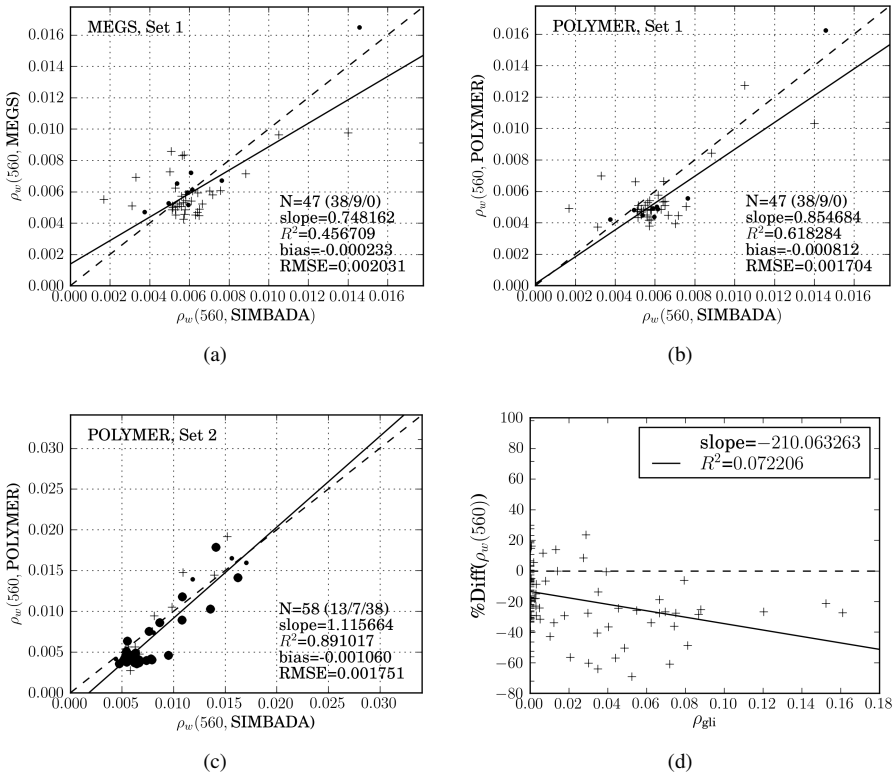

Fig. 8. Comparison between the *in situ* water reflectance from SIMBADA radiometer and the water reflectance estimated from MERIS data by the MEGS (Fig. (a)) and POLYMER (Fig. (b) for "set 1" and Fig. (c) for "set 2") algorithms, at 560 nm. In "set 1", HIGH_GLINT, PCD_1_13, cloudy and case 2 match-ups are rejected. In "set 2", only HIGH_GLINT or PCD_1_13 match-ups are included (cloudy and case 2 match-ups are still rejected). On these figures, the symbols "+", "·" and "•" represent respectively the flags "no glint", "medium glint" and "high glint", and the number of points N is differentiated in parentheses between these three classes. For "set 2", the relative percent difference between $\rho^+_{w,\text{POLYMER}}(490\text{nm})$ and $\rho^+_{wn,\text{INSITU}}(490\text{nm})$ is plotted against the reflectance of the sun glint ρ_{gli} (d). The relative percent difference between x_1 and x_2 if defined by $\%\text{Diff} = \frac{x_1 - x_2}{\frac{1}{2}(x_1 + x_2)}$.

				Comparison with SIMBADA				Correlation with ρ_{gli}	
Parameter	Processor	Set	N	slope	R^2	bias	RMSE	slope	R^2
$\rho_w^+(412)$	MEGS	1	39	0.79	0.863	-0.001521	0.005202		
	POLYMER	1	39	0.77	0.842	-0.003696	0.005571	-26.1	0.0004
	POLYMER	2	47	0.67	0.680	-0.001246	0.006499		
$\rho_w^+(443)$	MEGS	1	57	0.84	0.795	-0.001795	0.004685		
	POLYMER	1	57	0.80	0.861	-0.003168	0.004062	-52.1	0.004
	POLYMER	2	67	0.74	0.782	-0.002282	0.004787		
$\rho_w^+(490)$	MEGS	1	56	0.86	0.575	-0.001833	0.003120		
	POLYMER	1	56	0.86	0.697	-0.003162	0.002601	-82.6	0.015
	POLYMER	2	56	0.84	0.625	-0.003655	0.003031		
$\rho_w^+(510)$	MEGS	1	58	0.89	0.137	-0.000125	0.002386		
	POLYMER	1	58	0.89	0.319	-0.001751	0.001989	-162.0	0.057
	POLYMER	2	67	1.05	0.703	-0.002114	0.002418		
$\rho_w^+(560)$	MEGS	1	47	0.75	0.457	-0.000233	0.002031		
	POLYMER	1	47	0.85	0.618	-0.000812	0.001704	-210.1	0.072
	POLYMER	2	58	1.12	0.891	-0.001060	0.001751		
$\rho_w^+(620)$	MEGS	1	58	1.08	0.232	0.000202	0.000787		
	POLYMER	1	58	1.04	0.641	-0.000067	0.000477	-742.0	0.142
	POLYMER	2	67	1.25	0.810	-0.000221	0.000695		
Chlorophyll	MEGS	1	44	0.78	0.825	0.050391	0.207509		
concentration	POLYMER	1	44	1.06	0.934	0.050193	0.129277	-182.6	0.026
($\log_{10}$)	POLYMER	2	48	1.10	0.939	-0.063813	0.158026		

Table 2. The comparison between SIMBADA and MERIS processed with MEGS and POLYMER, done at 560 nm on Figs. 8a to 8c, is repeated for other wavelengths, and chlorophyll concentration. This table summarizes the corresponding statistical parameters (number of points, slope and correlation coefficient of the regression, accuracy and precision). The two last columns give the slope and correlation coefficient for the regression of the relative percent difference of POLYMER parameters (set 1 + set 2) against the reflectance of the sun glint, as by Fig. 8d

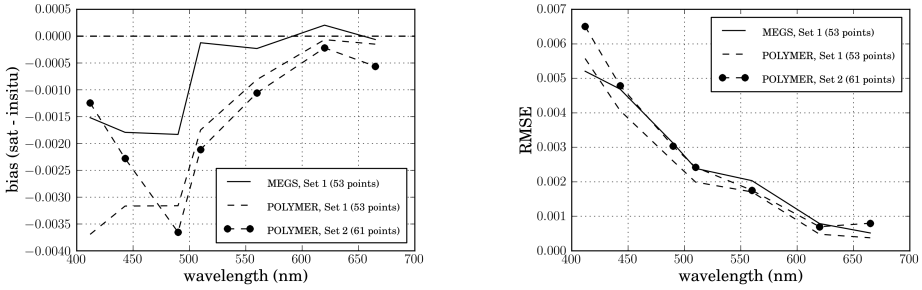

(a) (b)

Fig. 9. Plots of the accuracy (bias, Fig. 9a) and precision (RMSE, Fig. 9b) from the comparison between SIMBADA data and the water reflectances estimated from MERIS data using MEGS and POLYMER processors (see table 2), as a function of the wavelength.

The global gain in coverage makes it possible to obtain a very good monitoring of the ocean color parameters in composites of only 3 days. The robustness of POLYMER to the effects of the sun glint and semi-transparent clouds leads to a very large gain of spatial coverage — a factor greater than 2 compared to the standard MEGS product when the quality flag PCD_1_13 is discarded. This is a remarkable opportunity to monitor dynamic geophysical phenomenon over a shorter time period and increase the repetitiveness of the observations.

Acknowledgments

The authors would like to thank the MERMAID team for providing access to their database, and ESA for providing the MERIS data.